Soft Matter

View Online
Dynamic Article Links

Cite this: *Soft Matter*, 2011, **7**, 2879

www.rsc.org/softmatter

PAPER

Swelling behavior of nanoscale, shape- and size-specific, hydrogel particles fabricated using imprint lithography†

Mary Caldorera-Moore,[a] Min Kyoo Kang,[b] Zachary Moore,[a] Vikramjit Singh,[c] S. V. Sreenivasan,[c] Li Shi,[c] Rui Huang*[b] and Krishnendu Roy*[a]

Received 21st October 2010, Accepted 5th January 2011
DOI: 10.1039/c0sm01185a

Recently a number of hydrogel-based micro- and nanoscale drug carriers have been reported including top down fabricated, highly monodisperse nanoparticles of specific sizes and shapes. One critical question on such approaches is whether *in vivo* swelling of the nanoparticles could considerably alter their geometry to a point where the potential benefit of controlling size or shape could not be realized. Little has been reported on experimental characterization of the swelling behavior of nanoscale hydrogel structures, and current theoretical understanding is largely based on bulk hydrogel systems. Using atomic force microscopy (AFM) and environmental scanning electron microscopy (ESEM) capsules, we have characterized the swelling behavior of nano-imprinted hydrogel particles of different sizes and aspect ratios. Our results indicate a size-dependent swelling which can be attributed to the effect of substrate constraint of as-fabricated particles, when the particles are still attached to the imprinting substrate. Numerical simulations based on a recently developed field theory and a nonlinear finite element method were conducted to illustrate the constraint effect on swelling and drying behavior of substrate-supported hydrogel particles of specific geometries, and compared closely with experimental measurements. Further, we present a theoretical model that predicts the size-dependent swelling behavior for unconstrained sub-micron hydrogel particles due to the effect of surface tension. Both experimental and theoretical results suggest that hydrogel swelling does not significantly alter the shape and size of highly crosslinked nanoscale hydrogel particles used in the present study.

A. Introduction

The development of next-generation drugs, designed to interfere with specific cellular functions and pathways, has led to the demand for carriers that can efficiently and accurately deliver these agents to diseased cells or tissue while having minimal or no side effects. To accommodate this need, a significant amount of research efforts have been put into the development of micro- and nanoparticles for protecting sensitive biological agents, targeting specific sites or biological conditions, and for environmentally triggered controlled release of encapsulated agents. Hydrogels are cross-linked polymeric matrices that are widely utilized in a variety of biomedical applications primarily due to their high biocompatibility and their ability to be tailored for specific applications, including drug delivery.[1–17] Most micro- and nanoparticles for drug delivery are fabricated using "bottom-up" synthesis methods that often produce a poly-disperse population of particles. Recently, it has been postulated that particle size and shape can play an important role in *in vivo* transport and cellular uptake of the drug carriers.[18–23] This has led to significant efforts in developing top-down lithography methods for fabricating mono-disperse hydrogel particles of specific shape and size for drug delivery.[24–37] However, one critical issue that has not been addressed is whether *in vivo* swelling can alter the size and shape of these nanoscale hydrogel particles to a point that would compromise the potential benefit of the intended sizes and shapes.

Methods for evaluating bulk hydrogel properties are well established and have been widely reported.[3,38–45] However, whether the swelling behavior of nanoscale hydrogels correlates to the swelling properties of bulk hydrogels has yet to be investigated. This is partly because it is difficult to accurately measure particles at sub-500 nm dimensions under aqueous conditions and partly due to the fact that poly-disperse micro- and nanoscale particles synthesized using bottom up techniques consist of a population of particles of varying sizes. Conventional scanning

[a]*The University of Texas at Austin—Department of Biomedical Engineering, C0800, 1 University Station, BME 5.202B, Austin, TX, 78712, USA. E-mail: kroy@mail.utexas.edu*
[b]*The University of Texas at Austin—Department of Aerospace Engineering and Engineering Mechanics, Austin, TX, 78712, USA. E-mail: ruihuang@mail.utexas.edu*
[c]*The University of Texas at Austin—Department of Mechanical Engineering, Austin, TX, 78712, USA*

† Electronic supplementary information (ESI) available: Additional scanning electron microscopy and atomic force microscopy results. Full derivation of surface tension effects. See DOI: 10.1039/c0sm01185a

or transmission electron microscopy (SEM or TEM) techniques do not allow accurate measurement of hydrogel structures due to drying in vacuum as well as other effects caused by electron irradiation or the requirement of a metal coating layer. Further, evaluating nanoparticles in an aqueous environment is necessary to characterizing the hydrogel's structure in the swollen state; but due to resolution limitations of conventional microscopy techniques, it is difficult to measure.

Here we report both experimental and theoretical investigation on the swelling behavior of mono-disperse, nanoscale hydrogel particles fabricated using Step and Flash Imprint Lithography (S-FIL).[46] These nano-imprinted particles allow for precise control over particle geometries (shape, size and aspect ratios), thereby making it possible to evaluate the size effect on the swelling behavior compared to poly-disperse particles. Environmental scanning electron microscopy (ESEM) was used to study particle dimensions in aqueous suspension while atomic force microscopy (AFM) was employed to characterize changes in particle dimensions from the as-fabricated state to the swollen or dried state particles still attached to the imprinting surface.

ESEM of nanoparticle features was obtained using QuantomiX WETSEM® capsules that allow high resolution imaging of fully hydrated samples using standard SEM systems. Electron microscopy (EM) systems (SEM and TEM) are the primary method for high-resolution imaging of nanoscale features. Unfortunately, these systems require samples to be exposed to high vacuum and exposure to destructive electron beams. These drawbacks have limited the use of SEM for evaluation of polymer based hydrogel systems in their naïve state. The WETSEM® capsule contains a transparent membrane that completely isolates a wet sample from the SEM chamber environment (vacuum). The capsule membrane serves as the specimen holder that allows for electrons to enter and exit the capsule while maintaining the sample at atmospheric pressure.

Accurate and reproducible measurements of particle dimension required that AFM measurements be obtained with nanoparticles still attached to the imprinting surface, such that the particles orientation would not be random. However, under such constraint, the swelling profile is neither homogeneous nor isotropic. To address this and other limitations in current nanoscale metrology techniques, we present a theoretical model developed to understand the effects of surface tension and substrate constraint in the measurement results, and to predict the conditions for size-dependent swelling that cannot be resolved with current experimental measurement capabilities.

Hydrogel materials are composed of hydrophilic polymeric networks that are crosslinked into a matrix like network either by chemical bonds or physical entanglements.[38,41,47–51] Due to this mesh-like network, hydrogels have the ability to swell or shrink, altering the overall structure. Hydrogels are commonly characterized by three parameters: the polymer volume fraction in the swollen state, $v_{2,s}$, the number average molecular weight between cross-links, M_c, and the correlation length also known as the network pore (or mesh) size, ξ.[48] The equilibrium polymer volume fraction in the gel, $v_{2,s}$, is the ratio of the volume of the polymer ($V_{polymer}$) to the volume of the swollen gel (V_{gel}) and the reciprocal of the volume swelling ratio Q (relative to the dry polymer network).

For bulk hydrogels, the volume swelling ratio and polymer volume fraction in the swollen state can be measured through equilibrium swelling experiments.[48] The number-average molecular weight (M_c) and the pore size (ξ) can then be determined based on a theoretical model for swelling of polymer hydrogels.[52] Using a modified Flory–Rehner theory, Merrill and Peppas developed a theoretical framework that has significant success in describing the hydrogel swelling behavior.[38,49] Hilt *et al.* presented the complete derivation of the hydrogel characterization equation previously[48] that is summarized here.

A combination of thermodynamics and rubber elasticity theories states that a crosslinked polymer gel that is immersed in a fluid swells under two opposing forces: the thermodynamic force of mixing and the retractive force induced by the crosslinked polymer network. The swelling reaches equilibrium when these two forces are balanced. When the gel reaches equilibrium, the chemical potential inside the gel equals that of the pure solvent in the surrounding environment and thus the relative chemical potential is zero, based on which one obtains an expression for determining $\bar{M}_c$ in a neutral hydrogel:

$$\frac{1}{\bar{M}_c} = \frac{2}{\bar{M}_n} - \frac{\bar{v}}{V_1}\frac{\ln(1-v_{2,s}) + v_{2,s} + \chi v_{2,s}^2}{\left(v_{2,r}^{2/3} v_{2,s}^{1/3} - \frac{\kappa}{2} v_{2,s}\right)} \quad (1)$$

where V_1 is the molar volume of the solvent (*e.g.*, water), $v_{2,r}$ is the polymer volume fraction at the relaxed state (reference configuration), $\bar{v}$ is the specific volume of the polymer, k_B is the Boltzmann constant, $\bar{M}_n$ is the molecular weight of the linear polymer chains before cross-linking, and χ is a dimensionless parameter that is specific to the gel and characterizes the interaction between the solvent and the polymer. This equation can then be used to determine $\bar{M}_c$ from the measurements of equilibrium swelling ratio (Q) or the polymer volume fraction ($v_{2,s} = 1/Q$) in the swollen state. The dimensionless parameter κ equals 1 in the original theory but equals 2 in some modified theories.[53] We note that eqn (1) allows us to approximate the effective molecular weights between crosslinks ($\bar{M}_c$) based on experimentally measured swelling ratios. Although the underlying assumptions of the molecular structures made in this equation are more simplistic than our current system, nevertheless it provides a rational estimation for the current studies.

B. Materials and methods

Materials and reagents

Poly(ethylene glycol) diacrylate (PEGDA, M_w 700) was purchased from Sigma Aldrich. The ultraviolet (UV) photoinitiator, 2-hydroxy-1-[4-(hydroxyethoxy) phenyl]-2-methyl-1 propanone (I2959) was purchased from Ciba Geigy. Fluorescein-*o*-acrylate monomer (97%), poly(vinyl alcohol) (PVA, M_w 31 000) (Fluka), and dimethyl sulfoxide (DMSO) were purchased from Sigma Aldrich. Heptane was purchased from Fisher Scientific. TEM Grids (400 mesh Formvar/Carbon film grids), QuantomiX WETSEM® particle imaging kit, and QX-102 starter package were purchased from Electron Microscopy Sciences (EMS). High resolution focused ion beam (FIB) FIB2-100 2 μm tapping mode Si AFM probes were purchased from Veeco.

Hydrogel preparation

Hydrogel solutions for bulk and nanoscale hydrogel formulations were prepared from various percent polymer concentrations (% volume (v)) of poly(ethylene glycol) diacrylate (PEGDA) M_w 700 in deionized water (DH_2O). The UV photoinitiator, 2-hydroxyl-1-[4-(hydroxyl)phenyl]-2-methyl-1 propanone (I2959, Ciba), was used at concentrations below those previously determined to be cyto-compatible.[54] I2959 was dissolved in DH_2O in a concentrated amount and then a small amount was added to the PEGDA solution at a final concentration of 0.07% (w/w). Hydrogel solutions were also prepared with the fluorescent monomer fluorescein-*o*-acrylate to incorporate a contrast agent into the hydrogel network. The fluorescein-*o*-acrylate monomer was dissolved in dimethyl sulfoxide (DMSO) and then added to the PEGDA imprinting solution, at a final concentration of 2% (w/v); at a molar ratio of 1 : 0.45 PEGDA : fluorescein for the 50% (v) hydrogels and 1 : 0.64 molar ratio in the 33% (v) hydrogels.

Characterization of bulk hydrogel swelling

Bulk hydrogel discs were prepared from 500 μL of PEGDA 700 or PEGDA 700 containing fluorescein-*o*-acrylate hydrogel solutions at various concentrations of 10–50% (v) of the PEGDA macromer crosslinker were photopolymerized using UV at 365 nm wavelengths at an intensity of ~4 mW cm^{-2} for 20 minutes. Hydrogel discs were weighed in air as well as in heptane (a solvent the PEG hydrogels do not swell in) to obtain the volume of the hydrogels, immediately after UV-polymerization. The hydrogels were then rinsed for 24 hours in DH_2O (periodically changed) to remove any un-reacted polymer or monomer. Hydrogel discs were dried for 48 hours using a vacuum chamber and subsequently weighed to obtain dry (or polymer) mass. The dried gels were then swollen for 48 hours in DH_2O at 37 °C to reach swollen equilibrium. The polymer volume fraction in the swollen state, $\nu_{2,s}$, and relaxed state, $\nu_{2,r}$, was calculated from the measured hydrogel mass in air and in heptane:

$$\nu_{2,s} = \frac{W_{a,d} - W_{n,d}}{W_{a,s} - W_{n,s}} \quad (2)$$

$$\nu_{2,r} = \frac{W_{a,d} - W_{n,d}}{W_{a,r} - W_{n,r}} \quad (3)$$

where $W_{a,d}$ is the hydrogel weight in dry state in air, $W_{n,d}$ is the hydrogel weight in dry state in heptane, $W_{a,s}$ is the hydrogel weight in swollen state in air, $W_{n,s}$ is the hydrogel weight in swollen state in heptane, $W_{a,r}$ is the hydrogel weight in the relaxed state in air, and $W_{n,r}$ is the hydrogel weight in the relaxed state in heptane. The equilibrium volume swelling ratio (Q) was calculated by comparing the ratio of the equilibrium swollen volume with the polymer volume at the dry state.[3,48]

Evaluation of hydrogel nanoparticle morphology using SEM, TEM, ESEM, and AFM

Nanoscale hydrogel particles of various lengths with the same cross-section dimensions of 800 nm by 100 nm by 100 nm (811), 400 nm by 100 nm by 100 nm (411), and 100 nm by 100 nm by 100 nm (111), respectively, were fabricated using the Imprio 100 S-FIL system (Molecular Imprints, Austin TX). Nanoparticles composed of 50% (v) PEGDA and 2% (v/w) fluorescein-*o*-acrylate and 33% (v) PEGDA and 2% (v/w) fluorescein-*o*-acrylate were imprinted on wafers coated with the PVA water soluble release layer. In the studies presented here, the S-FIL process was modified to fabricate mono-disperse shape- and size-specific nanoparticles composed of poly (ethylene glycol) diacrylate (PEGDA). The process included design and fabrication of nanopatterned quartz imprinting templates, creation of an imprinting substrate that facilitates mild release of nanoparticles, characterization of biocompatible imprinting solutions, and optimization of the nano-imprinting process, using an Imprio 100 imprinting tool (Molecular Imprints, Austin TX). Detailed methods of nanoimprinting using the Imprio 100 and subsequent etching, and release of these shape- and size-specific nanoparticles have been previously reported[46] by our group. Briefly, a pre-patterned transparent quartz mold is pressed (12–30 Newtons) into polymer droplets inkjetted on silicon wafers pre-coated with an aqueous solution release layer (2% (w) PVA), causing it to spread, and fill the features in the mold. The polymer is then exposed to a short UV light pulse (at 365 nm wavelength at 5 mW cm^{-2} intensity, for 10 seconds) to photopolymerize. The quartz mold is then removed revealing the desired nanostructures. The residual layer of the imprints is first measured using NanoSpec AFT and/or SEM. A low power (50 Watts) oxygen plasma etch (Plasma Therm 790 Series Reactive Ion Etcher (RIE)) was performed at a pressure of 180 mTorr with O_2 (18 sccm) for 20–60 seconds depending on the residual thickness. AFM was used to verify that the imprinted particles retained their structure and shape after etching.

Nanoscale swelling studies using EM. After removal of the residual layer, particles were released in 0.22 μm filtered DH_2O. Imprints used for AFM studies were not released from the wafer, instead an adhesive layer (Transpin, Molecular Imprints) was used to keep particles adhered to the substrate. Particles from each group were placed on Si wafer pieces, allowed to dry, sputter coated with 8 nm of gold palladium, and then imaged using standard SEM methods with the LEO 1530 SEM. Particles from each group were also negatively stained with uranyl acetate on a copper mesh formvar TEM grid and TEM imaging was conducted using the FEI Tecnai Transmission Electron Microscope. Lastly, particles were incubated in filtered water for 24 hours to allow for the particles to reach equilibrium swelling, and then imaged using the QuantomiX water SEM capsules (QuantomiX Technologies). Prior to imaging, the capsule membranes were coated with 4 mg mL^{-1} polyethylenimine (PEI) (M_w 4000) solution to create a positively charged surface to promote adhesion of the nanoparticles (due to the oxygen plasma etching contain a negative surface charge) to the membrane. The membrane is incubated with PEI solution for 1 hour and is then rinsed 5 times with filtered DH_2O. Solutions containing particles were then added to the capsule and spun down for 5 minutes at 3000 rcfs. Capsules containing particles were then imaged using the LEO 1530 SEM using a Robinson back scattering detector. Prior to imaging the S-FIL particles, the SEM system was calibrated using the QuantomiX calibration sample containing particles of known dimensions that do not swell in the presence of water, to verify that the system was calibrated to correct dimensions for samples in water.

Nanoscale swelling studies using AFM. Particles composed of 50% (v) PEGDA and 2% (v/w) fluorescein-*o*-acrylate, and 33% (v) PEGDA and 2% (v/w) fluorescein-*o*-acrylate were imprinted on Transpin HE-0600 (Molecular Imprints) coated wafers to chemical cross-link the imprints to the substrate.

The residual layer formed between particles was removed with a low powered oxygen plasma etch for 20–40 seconds and subsequently imaged using AFM with a high resolution tip prepared by focused ion beam (FIB) milling, at a 512 by 512 line scan, to obtain nanoparticle topography after the fabrication process. The particles (still on the imprinting substrate) were then rinsed for 12 hours to remove any un-reacted polymer and monomer from the nanoparticles. The imprints were dried for 24 or 48 hours in a vacuum chamber and then immediately scanned to obtain the nanoparticle morphology in the dried state. Particles were then incubated in DH_2O for 24 or 48 hours and then imaged to obtain the particle topography in swollen state.

Statistical analysis. A *t*-distribution with a confidence level of 95% was used to evaluate the uncertainty of the measurements. All values presented here are reported as the total uncertainty that includes both the random errors for a sample size of 60 particles scanned and systematic errors due to AFM tip resolution and calibration.

C. Results and discussion

1. Bulk hydrogel swelling behavior

Bulk swelling behavior of hydrogels of different volume percent (v/v) polymer (poly (ethylene glycol) diacrylate (PEGDA), molecular weight (M_w) 700) was measured using standard swelling protocols reported previously.[3] The results are summarized in Table 1. The equilibrium swelling ratio decreased from 3.0 to 1.5 as the crosslink density increased. By varying the polymer concentration, equilibrium polymer volume fraction in the hydrogel ($\nu_{2,s}$) in the range of 0.33–0.65 was obtained. The number-average molecular weight between cross-links, M_c, as determined by eqn (1), decreased from 95.8 to 25.8 as the percent polymer fraction increased from 10 to 50% (v/v). This result is attributable to the fact that as the amount of polymer present for cross-linking in the hydrogel increases, the degree of cross-linking increases, thereby decreasing the average molecular weight between cross-links, which in turn increases the elastic stiffness of the network and decreases the equilibrium swelling ratio (Q). No significant difference was observed in bulk hydrogel properties between the pure PEGDA and PEGDA–fluorescein hydrogels. While the qualitative trend is reasonable, it is notable that the calculated values of M_c are low, suggesting that the structural assumptions underlying eqn (1) may not hold well for the specific hydrogels in the present study.

Table 1 Properties of bulk hydrogels of PEGDA (M_w 700). All values are calculated from averaged measured values

	$V_{2,r}$	$V_{2,s}$	M_c/g mol^{-1}	Q
PEGDA % (v)				
10	0.32	0.33	95.8	3.0
15	0.42	0.44	61.7	2.3
25	0.50	0.52	43.4	1.9
30	0.63	0.64	27.3	1.6
33	0.62	0.65	26.1	1.5
50	0.63	0.65	25.8	1.5
PEGDA % (v) + 2% (w) fluorescein				
33	0.71	0.65	30.3	1.5
50	0.56	0.67	27.0	1.5

2. Evaluation of nanoparticle swelling behavior

Nanoparticles of various shapes, composed of PEGDA (M_w 700) with fluorescein-*o*-acrylate, were produced using S-FIL as described previously.[46] To evaluate size and aspect ratio effects on nanoscale swelling, three particle dimensions were fabricated, including 100 nm by 100 nm by 100 nm (111), 400 nm by 100 nm by 100 nm (411), and 800 nm by 100 nm by 100 nm (811). In order to verify uniform particle fabrication, standard SEM was used to image the nanoimprinted PEGDA particles. Fig. 1 shows SEM images of 33% (v/v) particles before (A–C) and after (D–F) releasing from the imprint substrate (silicon wafer). It should be noted that standard SEM requires the specimen chamber to be under vacuum and thus only provides characterization of the hydrogel nanoparticles in the dry state. In addition, SEM or TEM imaging only provides two-dimensional analysis of the particles (length and width). When particle orientation becomes a variable as shown by TEM in Fig. 1G–I, the standard deviation of length, width, and area measurement increases (see ESI†). Thus SEM and TEM cannot be used for swelling analysis and have been used here to verify particle formation only.

3. Wet SEM measurements

To characterize the hydrogel nanoparticles containing fluorescein-*o*-acrylate at their wet swollen state, QuantmiX™ wet SEM capsules were used as an ESEM. Using these capsules, hydrogel nanoparticles can be imaged while in an aqueous environment. Fig. 2 demonstrates images obtained using these wet capsules. As shown, even with particles electrostatically attached to the capsule membrane, the particle orientation during imaging is random, making accurate length and width measurements difficult. Overall, the length and width values of the 50% (v/v) PEGDA 700 nanoparticles were smaller than the 33% (v/v) PEGDA 700 nanoparticles at the wet, swollen state. A significant increase in length and width was observed for the swollen nanoparticles in comparison to dried, released particles (see ESI† for averaged measured values). However, due to resolution limitations of this method, only the length of the particles (800 nm and 400 nm dimensions) but not width and height values (100 nm dimensions) of the particles were accurately measured.

4. AFM measurements

AFM can achieve better spatial resolution than SEM or ESEM and does not require a low pressure environment or samples to be coated with a conductive layer. Therefore, AFM was used to measure the dimension of 33% (v/v) and 50% (v/v) PEGDA 700 hydrogel nanoparticles of three different sizes and in three different states: as-fabrication, dry state, and swollen state. However, accurate and reproducible AFM measurement requires that the particles be immobilized onto a substrate. Thus,

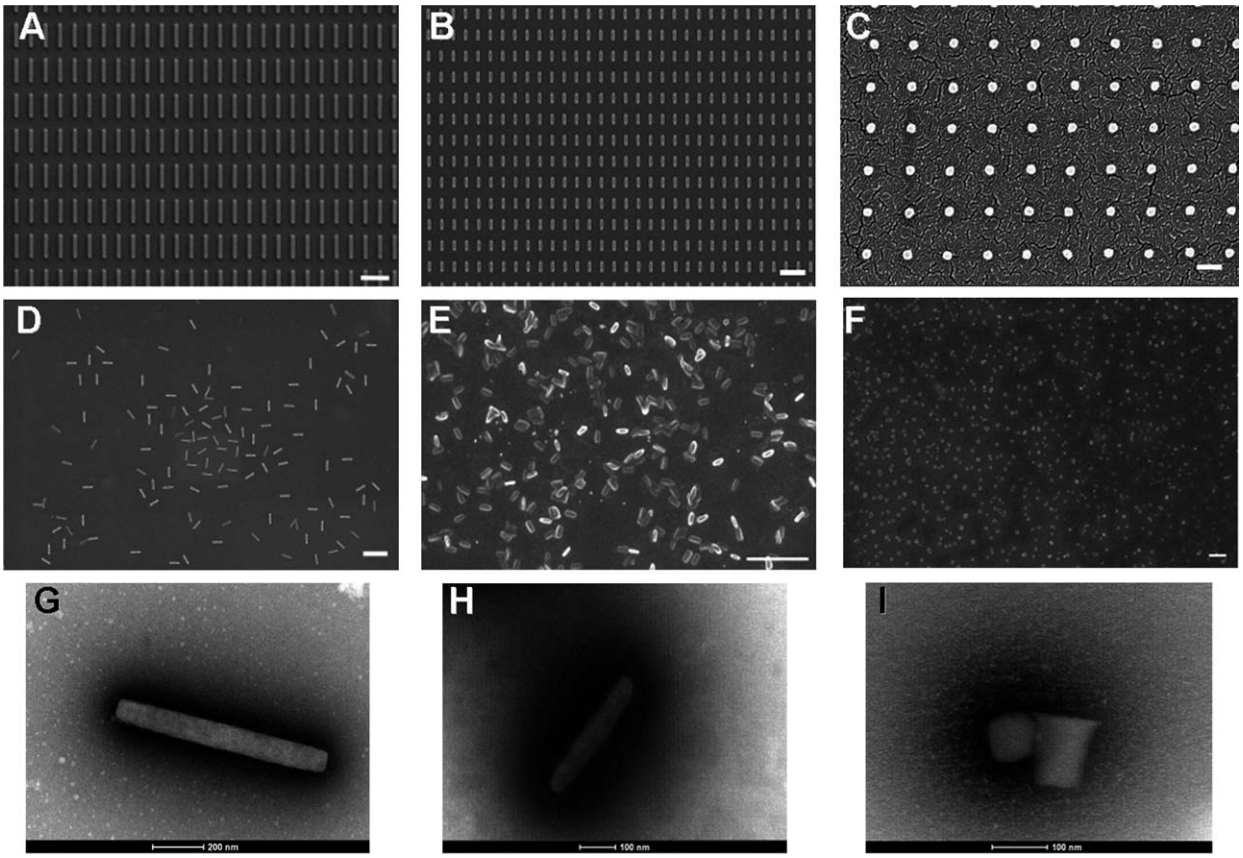

Fig. 1 S-FIL fabricated nanoparticles of various shapes and sizes. Imprints still on substrate: (A) 800 × 100 × 100 nm particles; (B) 400 × 100 × 100 nm particles; (C) 100 × 100 × 100 nm particles; released nanoparticles: (D) 800 × 100 × 100 nm particles; (E) 400 × 100 × 100 nm particles; (F) 100 × 100 × 100 nm particles. TEM of released particles: (G) 800 × 100 × 100 nm particles particle; (H) 400 × 100 × 100 nm particles; (I) 100 × 100 × 100 nm particles. (A, B, D, E and F) 2 micron scale bar, (C) 200 nm scale bar, (G) 200 nm scale bar and (H and I) 100 nm scale bar.

hydrogel particles adhered to the imprinting substrate were used for these studies. Fig. 3 shows typical AFM images and corresponding height profiles of imprinted particles still attached to the substrate. Fig. 4 presents average particle dimensions in each state for the 33% (v/v) PEGDA 700 hydrogel nanoparticles. As expected the particle dimensions (length, width and height) decreased when the particles were dried. Also as expected, the swollen particle's length and width increased. However, the AFM measured height slightly decreased at the swollen state in comparison to the relaxed and dry states. This unexpected behavior could be an artifact caused by the deformation of the swollen particles by the AFM probe as the hydrogel becomes softer after swelling. For this reason, the AFM measurement of heights is considered not as reliable as the measurements of length and width for the hydrogel particles.

5. A field theory and finite element method for inhomogeneous swelling of hydrogels

In order to understand the measurement results and to address the limitation of the experimental capability for measuring the swelling ratio of nanoparticles, we have developed a finite element method based on a field theory to analyze the nanoparticle swelling behavior. The standard theoretical treatment that led to eqn (1) for bulk swelling is limited by the assumption of isotropic and homogeneous swelling, which is independent of the particle size. Under geometric and mechanical constraints, however, a hydrogel particle may swell anisotropically and inhomogeneously, such as the hydrogel nanoparticles attached to the substrate for the AFM measurements in the present study. To understand inhomogeneous swelling of hydrogels, a field theory has been developed recently,[53,55] which incorporates the Flory–Rehner theory as the constitutive behavior of the hydrogel within a theoretical framework of nonlinear elasticity. Based on the field theory, a finite element method has been implemented to simulate inhomogeneous swelling of hydrogels.[55] Briefly, the nonlinear constitutive behavior of a hydrogel is specified by a user-defined material subroutine in a standard finite element package such as ABAQUS (ABAQUS (version 6.8), 2008; Dassault Systèmes Simulia Corp., Providence, RI, USA). The chemical potential of the hydrogel is mimicked by a temperature-like quantity in the user subroutine, which is set to be a constant in the hydrogel at the equilibrium state. Analogous to thermally induced deformation, change of the chemical potential leads to swelling or shrinking deformation of the hydrogel, subjected to the constraints by the prescribed boundary conditions. With such, both homogeneous and inhomogeneous swelling of hydrogels can be numerically analyzed as well as complex phenomena such as swell-induced surface creasing instability in confined hydrogels.[56]

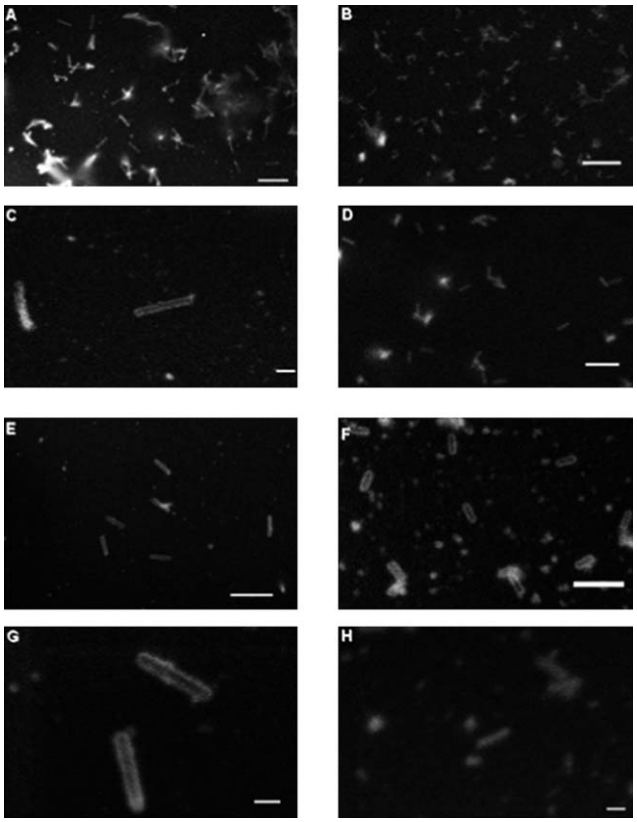

Fig. 2 Wet capsule SEM images. (A, C, E and G) 800 × 100 × 100 nm particles and (B, D, F and H) 400 × 100 × 100 nm particles. (A–D) 50% (v) hydrogel network and (E–H) 33% (v) hydrogel network. (A, B, E) 2 micron scale bar, (D and F) 1 micron scale bar, (C and G) 300 nm scale bar, and (H) 200 nm scale bar.

As discussed earlier, the Flory–Rehner theory as well as the modified forms (*e.g.*, the Peppas–Merrill equation in eqn (1)) is an approximation for the specific hydrogel materials in the present study. Nevertheless, as a common theoretical treatment, we present the theoretical treatise to illustrate the effects of substrate constraint and surface tension, which compares reasonably well with the experimental measurements in our study.

6. Effect of substrate constraint

For the hydrogel particles attached to the substrate for the AFM measurements, the effect of the substrate constraint leads to a size dependence for the swelling ratio. With the finite element method we simulate the drying and swelling deformation of the particles, using the material parameters determined from the bulk measurements (Table 1). The as-fabricated particles are taken as the relaxed state in a parallelepiped shape with the bottom surface fully constrained by the rigid substrate. Fig. 5 shows the results from the finite element simulation for one of the PEGDA particles, which is 400 nm by 100 nm by 100 nm at the relaxed state. In the dry state (Fig. 5a), the hydrogel particle has shrunk in all three dimensions. Due to the substrate constraint, however, the shrinking is inhomogeneous, as shown by the displacement contours. Similarly, in the swollen state (Fig. 5b), swelling is inhomogeneous. In both cases, the hydrogel particle

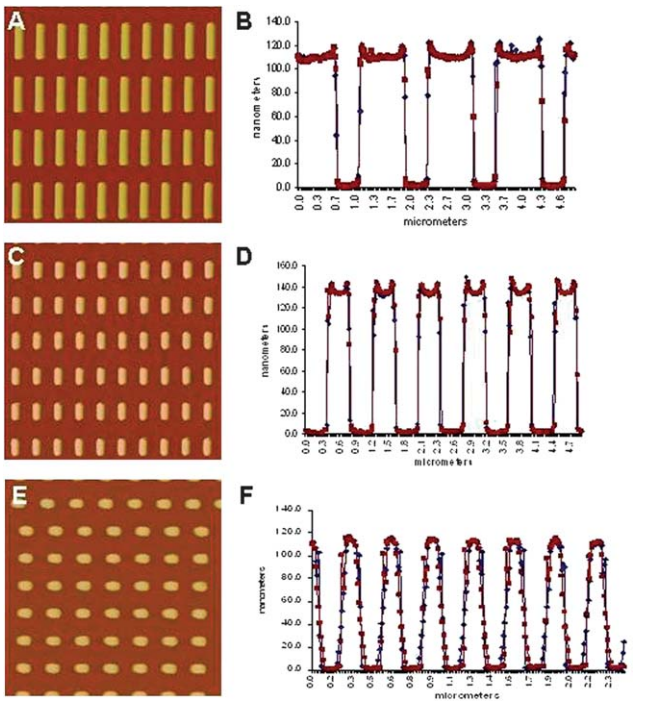

Fig. 3 AFM scans of 33% (v/v) PEGDA 700 S-FIL fabricated particles: (A and B) 800 × 100 × 100 nm particles, (C and D) 400 × 100 × 100 nm particles and (E and F) 100 × 100 × 100 nm particles. Scan tomography image: (A and C) 5 × 5 micrometre scan area and (E) 2.5 × 2.5 micrometre scan area. (B, D, and F) line scan of particle height profiles from AFM scan, where red is trace direction scan and blue is retrace direction scan.

deforms most significantly near the two ends, while the center part of the particle is highly constrained with little deformation in the length direction. The extension of the end deformation scales with the height of the particle. As a result, the effect of substrate constraint is stronger for longer particles, and the length swelling ratio increases as the particle size decreases.

Fig. 6 plots the calculated swelling (or shrinking) ratio in the length direction, relative to the relaxed state, for the three particle sizes in the present study. The lengths in the swollen state and the dry state are calculated from the finite element simulations, taking the average from the bottom to the top surface of each particle. Clearly, as the particle length increases, the relative deformation at both the dry and swollen states decreases, with the length ratio approaching 1. On the other hand, the swelling ratios for the swollen and dry states approach the upper and lower bounds set by unconstrained free particles as the particle length decreases, due to decreasing substrate constraint effect. To compare with the experimental data by AFM, we calculate the length swelling ratio (Q_{length}) as the ratio between the length in the swollen state and the length in the dry state, as discussed later (Fig. 8).

7. Effect of surface tension

For the released (unconstrained) hydrogel particles, another size effect is predicted theoretically by considering the effect of surface tension (see ESI† for full derivation). By considering the contribution of a surface free energy (or interface free energy),

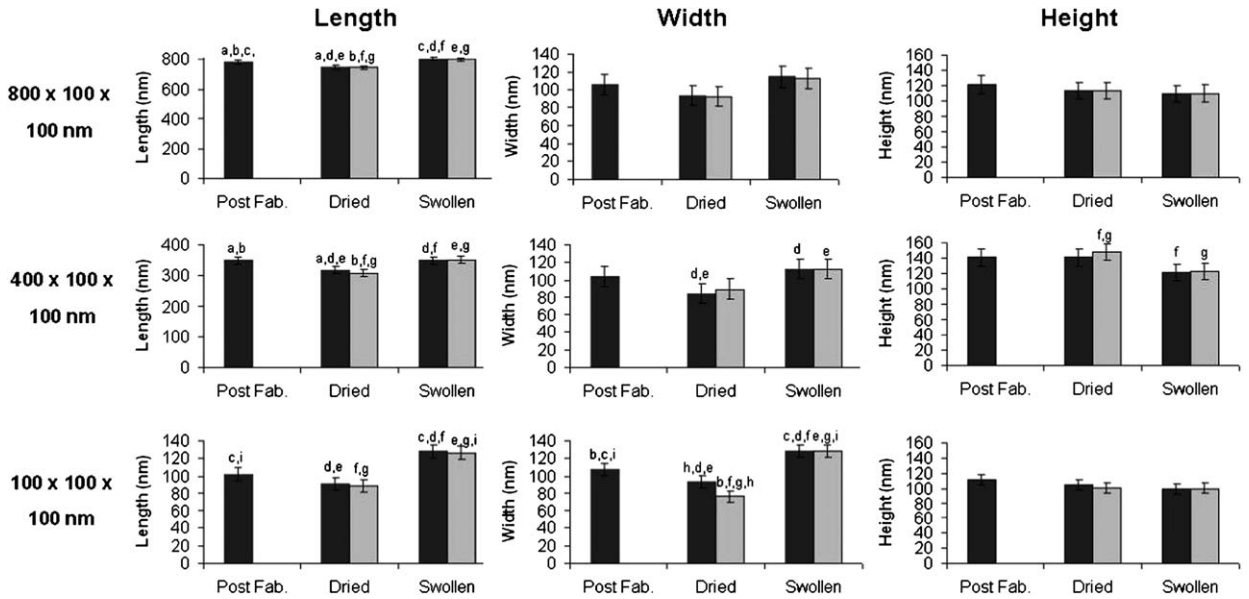

Fig. 4 33% (v/v) PEGDA 700 hydrogel nanoparticle topography values obtained using AFM, 24 hours later (black) and 48 hours later (grey). Data are plotted as average measured value ($n = 60$) and the error bars represent the total measurement uncertainty including both the systematic error due to the AFM resolution and random uncertainty. Match letters indicate values that are different outside the range of total uncertainty.

the polymer volume fraction at the equilibrium swollen state of a hydrogel particle can be obtained from the following equation:

$$\left[\ln(1-v_{2,s})+v_{2,s}+\chi v_{2,s}^2+\frac{V_1}{\bar{v}\bar{M}_c}\left(1-\frac{2\bar{M}_c}{\bar{M}_n}\right)\left(v_{2,r}^{2/3}v_{2,s}^{1/3}-\frac{\kappa}{2}v_{2,s}\right)\right] + \frac{2V_1\gamma}{3RT}\frac{S_0}{V_0}\left(\frac{v_{2,s}}{v_{2,r}}\right)^{1/3}=0 \quad (4)$$

where γ is the surface energy density (or surface tension), S_0 is the surface area in the relaxed state, V_0 is the volume of the hydrogel at the relaxed state, and R is the molar gas constant. The surface tension of a hydrogel may also be considered as the interfacial tension (or equivalently, interface energy density) between a hydrogel and its environment (*e.g.*, water, vapor, and other liquid). The terms in the first bracket of eqn (4) are the same for the bulk swelling in eqn (1). The last term on the left hand side of eqn (4) is due to the effect of surface tension. An intrinsic length scale of the hydrogel can be defined as:

$$L=\frac{2V_1\gamma}{3RT} \quad (5)$$

and a characteristic size of the particle is:

$$D_0=\frac{V_0}{S_0} \quad (6)$$

The effect of surface tension thus increases as the ratio, L/D_0, increases. For a large particle, since the ratio L/D_0 is negligibly small, the equilibrium swelling ratio is independent of the size. For a nanoscale hydrogel particle, the swelling ratio becomes size dependent.

To be specific, the following values are used for the hydrogels in the present study: $V_1 = 1.81 \times 10^{-5}$ m^3 mol^{-1}, $v = 7.88 \times 10^{-7}$ m^3 g^{-1}, $M_n = 700$ g mol^{-1}, and $\chi = 0.426$. From the

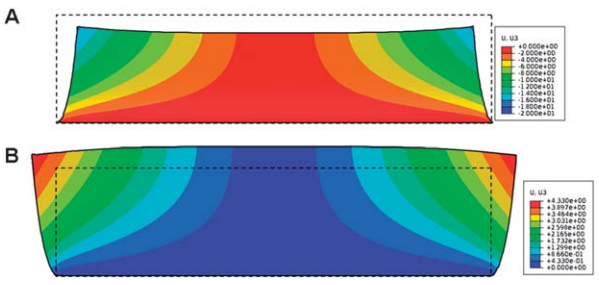

Fig. 5 Effect of substrate constraint: (A) dry state and (B) swollen state. The rectangular box outlined by the dashed lines shows the shape at the as-fabricated, relaxed state. The color contours show the displacement in the length direction, relative to the relaxed state.

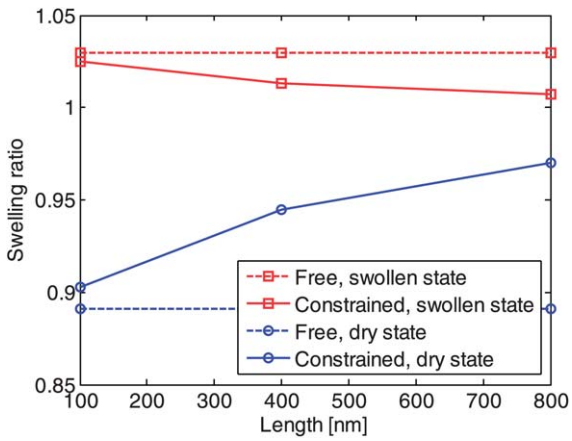

Fig. 6 Average length swelling ratio of hydrogel particles *versus* the length of particle, obtained from finite element calculations. The swelling ratio is relative to the relaxed state. The two horizontal dashed lines represent the upper and lower bounds, corresponding to free swelling and drying without the substrate constraint.

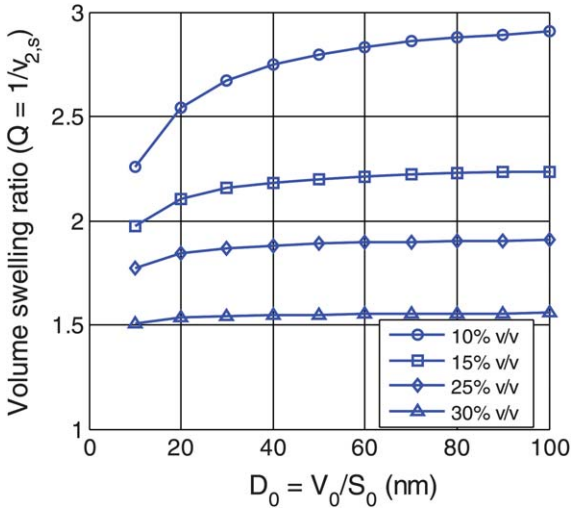

Fig. 7 Effect of surface tension on volume swelling ratio of hydrogels: corresponding to four different crosslink densities as listed in Table 1 (10–30% v/v, the results for 33% and 50% v/v PEGDA particles are nearly identical to that for 30% v/v PEGDA).

measurements of the bulk swelling ratios ($v_{2,r}$ and $v_{2,s}$ in Table 1), the molecular weight between crosslinks (M_c) is determined using eqn (1). The same parameters are then used to predict the volume swelling ratio for nanoscale hydrogel particles by eqn (3). For this purpose, we take the surface tension of water ($\gamma \approx 0.073$ N m^{-1}) as a rough estimate for the hydrogel.[57] We note that this value may be considered as an upper-bound estimation for surface tension of hydrogels immersed in water or vapor. By eqn (4), we obtain the intrinsic length scale $L \approx 0.34$ nm at $T = 310$ K (37 °C). Fig. 7 plots the predicted volume swelling ratio ($Q = 1/v_{2,s}$) as a function of the characteristic size (D_0) of the hydrogel particles. For the hydrogel particles of three different sizes in the present study (800 × 100 × 100 nm, 400 × 100 × 100 nm, and 100 × 100 × 100 nm), the characteristic sizes (D_0) are 23.5 nm, 22.2 nm, and 16.7 nm, respectively. Compared to the bulk hydrogel, the volume swelling ratio decreases as D_0 decreases. The effect of surface tension quantitatively depends on the molecular weight (M_c), which is stronger for the hydrogel particles with larger molecular weights. For PEGDA with 30% (v/v) and above, M_c is relatively small and the size effect is negligible even with the relatively large value for the surface tension used in this analysis. This qualitatively agrees with the SEM measurements of the released PEGDA particles.

8. Comparison of experimental and modeling results

As mentioned earlier, since only the length measurements were accurately discernible in wet ESEM studies and the change in length was the only parameter accurately measured using AFM, the swelling ratio in the length dimension (Q_{length}) at the nanoscale was determined and compared to the bulk Q_{length} (calculated) and the predicted Q_{length} from finite element analyses. As shown in Fig. 8, the Q_{length} calculated from the length dimensions of the 811 and 411 particles acquired using ESEM are comparable (within the margin of uncertainty) to the Q_{length} of bulk samples. This is in agreement with the model prediction shown in

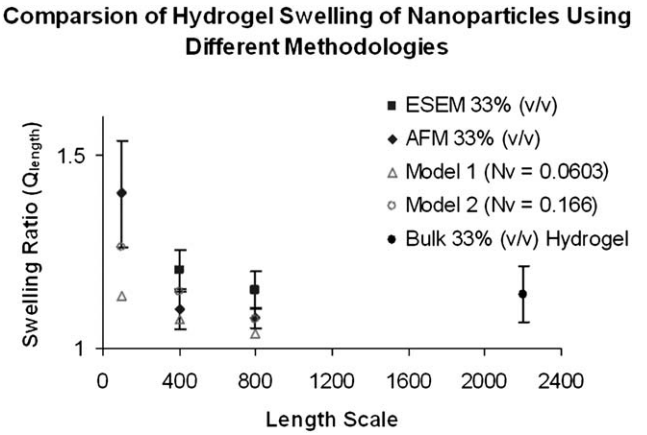

Fig. 8 Comparison of length swelling ratios from experimental measurements and finite element models. Experimental data presented as Q_{length} calculated from the averaged length values and the error bars are the calculated uncertainty in a total of 25 and 75 measurements for ESEM and AFM, respectively.

Fig. 7, where the effect of surface tension becomes appreciable only for hydrogel particles with low crosslink densities. Comparing the AFM and ESEM results, we see that the length swelling ratio decreases due to the effect of substrate constraint in the AFM measurements. Further, the AFM results show that the Q_{length} decreases as the length of the constrained particles increases. This qualitatively agrees with the finite element calculations for the substrate-constrained particles. The two finite element models (Model 1 and Model 2) in Fig. 8 represent hydrogel particles with two different molecular weights ($M_c \approx N_v$). Comparison of the experimental results from ESEM and AFM measurements to the computation modeling results demonstrates the effects of the constraint on the swelling ratio of the nanoparticles, although the measurement uncertainty is increasingly large for small particles.

D. Conclusions

Based on this series of *in vitro* hydrogel swelling studies conducted on both bulk and imprinted, monodisperse nanoscale hydrogels composed of various percent polymers 10–50% (v/v) PEGDA, the length swelling ratio is comparable to the bulk value when the length of the particle is longer than 400 nm while the width and height were 100 nm. From the experimental data, it also appears that once all three dimensions of the particles moves into the 100 nm size range the swelling ratio becomes significantly larger than the bulk value. The results from the 100 nm particles support the hypothesis that there could be size-dependent swelling behavior when the nanoparticle dimensions are 100 nm or below; but further investigation of sub-100 nm hydrogel particles is needed to confirm this. Based on a field theory and FEM analyses, this behavior is attributed to the effect of substrate constraint. Theoretical analysis of the hydrogel swelling behavior results further demonstrate that the highly crosslinked PEGDA M_w 700 hydrogels do not swell significantly, and therefore the shape and size of these specific top-down fabricated nano-carriers can be preserved in aqueous environments (*in vitro* and *in vivo* settings) for particle size larger than 100 nm. These results provide important guidelines for designing

top-down fabricated hydrogel nanoparticles with specific size and shape for enhancing the drug delivery efficacy.

Acknowledgements

This study was partially supported through the National Institutes of Health (Grant no. EB008835) and the National Science Foundation (Grant no. CMMI 0900715). RH and MKK gratefully acknowledge financial support by National Science Foundation through Grant No. 0547409.

References

1 M. Caldorera-Moore and N. A. Peppas, *Adv. Drug Delivery Rev.*, 2009, **61**, 1391–1401.
2 A. M. Lowman, M. Morishita, M. Kajita, T. Nagai and N. A. Peppas, *J. Pharm. Sci.*, 1999, **88**, 933–937.
3 S. J. Bryant and K. S. Anseth, *J. Biomed. Mater. Res.*, 2002, **59**, 63–72.
4 S. J. Bryant, R. J. Bender, K. L. Durand and K. S. Anseth, *Biotechnol. Bioeng.*, 2004, **86**, 747–755.
5 M. E. Byrne, K. Park and N. A. Peppas, *Adv. Drug Delivery Rev.*, 2002, **54**, 149–161.
6 D. Seliktar, A. H. Zisch, M. P. Lutolf, J. L. Wrana and J. A. Hubbell, *J. Biomed. Mater. Res., Part A*, 2004, **68**, 704–716.
7 D. T. Eddington and D. J. Beebe, *Adv. Drug Delivery Rev.*, 2004, **56**, 199–210.
8 A. L. Gonzalez, A. S. Gobin, J. L. West, L. V. McIntire and C. W. Smith, *Tissue Eng.*, 2004, **10**, 1775–1786.
9 S. Kim and K. E. Healy, *Biomacromolecules*, 2003, **4**, 1214–1223.
10 M. P. Lutolf, J. L. Lauer-Fields, H. G. Schmoekel, A. T. Metters, F. E. Weber, G. B. Fields and J. A. Hubbell, *Proc. Natl. Acad. Sci. U. S. A.*, 2003, **100**, 5413–5418.
11 F. Madsen and N. A. Peppas, *Biomaterials*, 1999, **20**, 1701–1708.
12 B. K. Mann, A. S. Gobin, A. T. Tsai, R. H. Schmedlen and J. L. West, *Biomaterials*, 2001, **22**, 3045–3051.
13 N. A. Peppas, J. Z. Hilt, A. Khademhosseini and R. Langer, *Adv. Mater.*, 2006, **18**, 1345–1360.
14 Y. Park, M. P. Lutolf, J. A. Hubbell, E. B. Hunziker and M. Wong, *Tissue Eng.*, 2004, **10**, 515–522.
15 N. A. Peppas, P. Bures, W. Leobandung and H. Ichikawa, *Eur. J. Pharm. Biopharm.*, 2000, **50**, 27–46.
16 K. Podual, F. J. Doyle and N. A. Peppas, *J. Controlled Release*, 2000, **67**, 9–17.
17 D. Seliktar, A. H. Zisch, M. P. Lutolf, J. L. Wrana and J. A. Hubbell, *J. Biomed. Mater. Res., Part A*, 2004, **68**, 704–716.
18 P. Decuzzi, F. Causa, M. Ferrari and P. A. Netti, *Ann. Biomed. Eng.*, 2006, **34**, 633–641.
19 P. Decuzzi and M. Ferrari, *Biomaterials*, 2006, **27**, 5307–5314.
20 P. Decuzzi, S. Lee, B. Bhushan and M. Ferrari, *Ann. Biomed. Eng.*, 2005, **33**, 179–190.
21 P. Decuzzi, R. Pasqualini, W. Arap and M. Ferrari, *Pharm. Res.*, 2009, **26**, 235–243.
22 J. A. Champion and S. Mitragotri, *Proc. Natl. Acad. Sci. U. S. A.*, 2006, **103**, 4930–4934.
23 J. A. Champion and S. Mitragotri, *Pharm. Res.*, 2009, **26**, 244–249.
24 L. E. Euliss, C. M. Welch, B. W. Maynor, J. P. Rolland, G. M. Denison, S. E. Gratton, J.-Y. Park, A. A. Pandya, E. L. Enlow, R. L. Juliano, K. M. Hahn and J. M. DeSimone, in *Advances in Resist Technology and Processing XXIII*, SPIE, San Jose, CA, USA, 2006, pp. 61534–61538.
25 S. E. A. Gratton, P. D. Pohlhaus, J. Lee, J. Guo, M. J. Cho and J. M. DeSimone, *J. Controlled Release*, 2007, **121**, 10–18.
26 S. E. A. Gratton, P. A. Ropp, P. D. Pohlhaus, J. C. Luft, V. J. Madden, M. E. Napier and J. M. DeSimone, *Proc. Natl. Acad. Sci. U. S. A.*, 2008, **105**, 11613–11618.
27 K. B. Wiles, N. S. Wiles, K. P. Herlihy, B. W. Maynor, J. P. Rolland and J. M. deSimone, *Soft lithography using perfluorinated polyether molds and PRINT technology for fabrication of 3-D arrays on glass substrates*, 2006; J. L. Michael (ed), SPIE: 2006, p. 61513F.
28 A. A. Pandya, B. W. Maynor, S. E. A. Gratton, D. G. Vellenga, D. G. Yu, C. M. Osburn and J. M. DeSimone, in *Emerging Lithographic Technologies X*, SPIE, San Jose, CA, USA, 2006, pp. 61513–61516.
29 J. P. Rolland, B. W. Maynor, L. E. Euliss, A. E. Exner, G. M. Denison and J. M. DeSimone, *J. Am. Chem. Soc.*, 2005, **127**, 10096–10100.
30 A. C. Dorian, P. H. Kevin and M. D. Joseph, *Wiley Interdiscip. Rev.: Nanomed. Nanobiotechnol.*, 2009, **1**, 391–404.
31 S. Gratton, M. Napier, P. Ropp, S. Tian and J. DeSimone, *Pharm. Res.*, 2008, **25**, 2845–2852.
32 J. Y. Kelly and J. M. DeSimone, *J. Am. Chem. Soc.*, 2008, **130**, 5438–5439.
33 S. L. Tao and T. A. Desai, *J. Assoc. Lab. Autom.*, 2004, **9**, 155–158.
34 S. L. Tao, K. Popat and T. A. Desai, *Nat. Protocols*, 2007, **1**, 3153–3158.
35 S. L. Tao and T. A. Desai, *Adv. Mater.*, 2005, **17**, 1625–1630.
36 L. Leoni and T. A. Desai, *Adv. Drug Delivery Rev.*, 2004, **56**, 211–229.
37 S. L. Tao and T. A. Desai, *Adv. Drug Delivery Rev.*, 2003, **55**, 315–328.
38 N. A. Peppas and E. W. Merrill, *J. Appl. Polym. Sci.*, 1977, **21**, 1763–1770.
39 C. S. Brazel and N. A. Peppas, *Macromolecules*, 1995, **28**, 8016–8020.
40 C. L. Bell and N. A. Peppas, *Biomaterials*, 1996, **17**, 1203–1218.
41 N. A. Peppas, Y. Huang, M. Torres-Lugo, J. H. Ward and J. Zhang, *Annu. Rev. Biomed. Eng.*, 2000, **2**, 9–29.
42 R. W. Korsmeyer and N. A. Peppas, *J. Membr. Sci.*, 1981, **9**, 211–227.
43 J. Berger, M. Reist, J. M. Mayer, O. Felt, N. A. Peppas and R. Gurny, *Eur. J. Pharm. Biopharm.*, 2004, **57**, 19–34.
44 K. S. Anseth, C. N. Bowman and L. Brannon-Peppas, *Biomaterials*, 1996, **17**, 1647–1657.
45 N. A. Peppas, K. B. Keys, M. Torres-Lugo and A. M. Lowman, *J. Controlled Release*, 1999, **62**, 81–87.
46 L. C. Glangchai, M. Caldorera-Moore, L. Shi and K. Roy, *J. ControlledRelease*, 2008, **125**, 263–272.
47 A. Lowman and N. Peppas, Hydrogels, in *Encyclopedia of Controlled Drug Delivery*, ed. E. Mathiowitz, Wiley, New York, 1999, pp. 397–418.
48 J. Z. Hilt, A. Khademhosseini, R. Langer and N. A. Peppas, *Adv. Mater.*, 2006, **18**, 1345–1360.
49 N. A. Peppas and E. W. Merrill, *J. Polym. Sci., Polym. Chem. Ed.*, 1976, **14**, 459–464.
50 J. Kopecek, *J. Polym. Sci., Part A: Polym. Chem.*, 2009, **47**, 5929–5946.
51 J. Kopecek, *Mol. Pharmaceutics*, 2010, **7**, 922–925.
52 P. J. Flory, *Principles of Polymer Chemistry*, 1953.
53 W. Hong, X. Zhao, J. Zhou and Z. Suo, *J. Mech. Phys. Solids*, 2008, **56**, 1779–1793.
54 S. J. Bryant, C. R. Nuttelman and K. S. Anseth, *J. Biomater. Sci., Polym. Ed.*, 2000, **11**, 439–457.
55 M. K. Kang and R. Huang, *J. Appl. Mech.*, 2010, **77**, 061004.
56 M. K. Kang and R. Huang, *Mech. Phys. Solids*, 2010, **58**, 1582–1598.
57 T. Nakamura, M. Hattori, H. Kawasaki, K. Miyamoto, M. Tokita and T. Komai, *Phys. Rev. E: Stat. Phys., Plasmas, Fluids, Relat. Interdiscip. Top.*, 1996, **54**, 1663.